Neuron
Article

Sensorineural Deafness and Seizures in Mice Lacking Vesicular Glutamate Transporter 3

Rebecca P. Seal,[1] Omar Akil,[2] Eunyoung Yi,[3] Christopher M. Weber,[2] Lisa Grant,[3] Jong Yoo,[4] Amanda Clause,[5] Karl Kandler,[5] Jeffrey L. Noebels,[4] Elisabeth Glowatzki,[3] Lawrence R. Lustig,[2] and Robert H. Edwards[1,*]
[1]Departments of Physiology and Neurology
[2]Department of Otolaryngology
School of Medicine, University of California, San Francisco, San Francisco, CA 94143, USA
[3]Department of Otolaryngology, Head and Neck Surgery, Johns Hopkins School of Medicine, Baltimore, MD 21205, USA
[4]Department of Neurology, Baylor College of Medicine, Houston, TX 77030, USA
[5]Departments of Otolaryngology and Neurobiology, University of Pittsburgh School of Medicine, Pittsburgh, PA 15261, USA
*Correspondence: robert.edwards@ucsf.edu
DOI 10.1016/j.neuron.2007.11.032

SUMMARY

The expression of unconventional vesicular glutamate transporter VGLUT3 by neurons known to release a different classical transmitter has suggested novel roles for signaling by glutamate, but this distribution has raised questions about whether the protein actually contributes to glutamate release. We now report that mice lacking VGLUT3 are profoundly deaf due to the absence of glutamate release from hair cells at the first synapse in the auditory pathway. The early degeneration of some cochlear ganglion neurons in knockout mice also indicates an important developmental role for the glutamate released by hair cells before the onset of hearing. In addition, the mice exhibit primary, generalized epilepsy that is accompanied by remarkably little change in ongoing motor behavior. The glutamate release conferred by expression of VGLUT3 thus has an essential role in both function and development of the auditory pathway, as well as in the control of cortical excitability.

INTRODUCTION

Synaptic transmission mediated by glutamate requires transport of the excitatory amino acid into secretory vesicles by a family of three vesicular glutamate transporters (VGLUTs) (Fremeau et al., 2004b; Takamori, 2006). Since all cells contain glutamate for its role in protein biosynthesis and intermediary metabolism, VGLUT expression thus appears to define neurons that release glutamate as a neurotransmitter. Consistent with this, heterologous expression of VGLUT1 and -2 in inhibitory neurons suffices to confer regulated glutamate release (Takamori et al., 2000, 2001). In addition, analysis of VGLUT expression patterns has revealed a number of neuronal populations not previously thought to release glutamate (Boulland et al., 2004; Gras et al., 2005).

The three VGLUT isoforms exhibit a mutually exclusive distribution in the adult brain, suggesting a distinct role for each protein. VGLUT1 and -2 are the predominant isoforms and together include essentially all of the neurons previously shown to release glutamate as a transmitter (Fremeau et al., 2001; Herzog et al., 2001; Kaneko et al., 2002; Varoqui et al., 2002). In contrast, VGLUT3 is expressed by neuronal populations that are usually associated with the release of a transmitter other than glutamate, such as serotonergic neurons in the dorsal and medial raphe nuclei and cholinergic interneurons in the striatum (Fremeau et al., 2002; Gras et al., 2002; Schafer et al., 2002). In the hippocampus and cortex, VGLUT3 is expressed by GABAergic interneurons that form perisomatic, symmetric synapses usually associated with inhibitory transmission (Fremeau et al., 2002). In addition, VGLUT3 has been detected outside the nervous system in liver, kidney, and muscle (Boulland et al., 2004; Fremeau et al., 2002; Gras et al., 2002; Schafer et al., 2002).

VGLUT3 also differs markedly from the other two isoforms in its membrane trafficking (Voglmaier et al., 2006). VGLUT1 and -2 rely on distinct interactions with the endocytic machinery for recycling but remain almost exclusively axonal. In contrast, VGLUT3 can target to the cell body and dendrites, as well as the axon of certain neurons (Fremeau et al., 2002; Gras et al., 2002), and has been implicated in the retrograde synaptic release of glutamate (Harkany et al., 2004).

The unusual distribution of VGLUT3 has suggested novel roles for signaling by glutamate. Although the three isoforms exhibit similar transport activity using in vitro assays, heterologous expression of VGLUT3 in neurons has not conferred detectable postsynaptic responses to glutamate (Takamori et al., 2000, 2001), raising questions about whether the protein actually contributes to glutamate release. We therefore produced mice lacking VGLUT3 and now report that the transporter indeed mediates the regulated exocytosis of glutamate and as such has a critical role in both the auditory pathway and the control of cortical excitability.

RESULTS

To determine the physiological role of VGLUT3, we produced mice that lack the transporter by homologous recombination in mouse embryonic stem cells, deleting the first transmembrane domain and lumenal loop of the protein (Figure 1A). Disruption of the gene was confirmed by Southern analysis and PCR, and the loss of VGLUT3 protein was confirmed by immunostaining

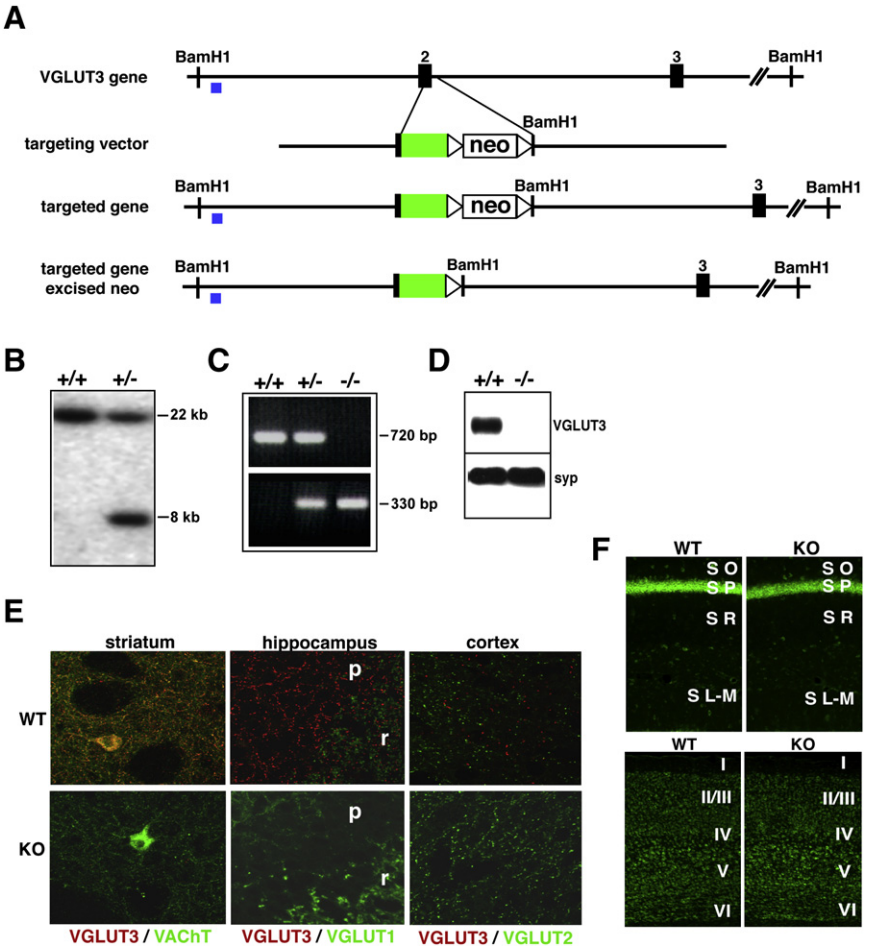

Figure 1. Targeted Disruption of the VGLUT3 Locus

(A) Restriction maps of the WT VGLUT3 mouse gene locus, the targeting construct, and the properly recombined allele. In the recombined allele, most of exon 2 is replaced by EGFP (green box) and the positive selectable marker for resistance to neomycin (neo). The neo gene, flanked by loxP sites, was deleted by mating mice heterozygous for VGLUT3 to β-actin-cre mice that express cre recombinase in the germline. Exon 2 encodes the first transmembrane domain and part of the first lumenal loop of VGLUT3, including glycosylation sites. The 5′ probe (blue box) used to identify properly targeted ES cell clones resides upstream of the left arm.

(B) Southern blot of BamH1-cut genomic DNA from three neomycin-resistant ES cell clones. The wild-type allele results in an ~22 kb band, whereas the targeted allele results in an ~8 kb fragment.

(C) PCR amplification of genomic tail DNA from wild-type (+/+), heterozygous (+/−), and homozygous (−/−) VGLUT3 knockout (KO) mice. A 720 bp band is amplified from the wild-type allele, and a 330 bp band from the recombined allele.

(D) Western blot of crude brain synaptic vesicles prepared from wild-type (+/+) and VGLUT3 KO (−/−) littermates probed with antibodies to VGLUT3 and synaptophysin (syp).

(E) Striatal, hippocampal, and cortical slices from wild-type (WT) and VGLUT3 KO mice were immunostained for VGLUT3 (red) and VAChT, VGLUT1, or VGLUT2 (all green).

(F) Hippocampal region CA1 (top) and parietal cortex (bottom) of VGLUT3 KO mice show no difference from WT in overall morphology assessed by Nissl stain (green).

brain sections and immunoblotting brain extracts (Figures 1B–1E). VGLUT3 knockout (KO) mice are born in the expected Mendelian ratios and do not exhibit any obvious anatomic or motor abnormalities. Brain architecture as well as the number and morphology of neuronal populations known to express VGLUT3 show no obvious difference from wild-type (WT) littermates (Figures 1E and 1F and data not shown).

Sensorineural Deafness in VGLUT3 Knockout Mice

VGLUT3 is expressed during development by a population of GABAergic neurons in the auditory brainstem pathway where it may contribute to the tonotopic refinement required for sound localization (Gillespie et al., 2005). VGLUT3 KO mice might therefore be expected to exhibit a subtle deficit in auditory acuity. However, the mice do not startle in response to even a loud clap. To quantify their response to sound, we used acoustic startle chambers. As shown in Figure 2A, VGLUT3 KO animals show no startle to sound as loud as 125 dB, whereas WT littermates exhibit a robust startle at much lower intensities. On the other hand, VGLUT3 KO mice show a normal righting reflex and performance on the rotorod (data not shown), suggesting normal motor and vestibular function.

Since the absence of startle to sound could reflect an impairment of pathways not related specifically to hearing, we assessed auditory function more directly. The auditory brainstem response (ABR) measures evoked potentials time-locked to the onset of sound at synapses along the auditory pathway, starting with the inner hair cell (IHC)-auditory nerve synapse. VGLUT3 KO mice and WT littermates were subjected on postnatal day 21 (P21) to broadband clicks at intensities ranging from 23.1 to 91.5 dB sound pressure level (SPL). In contrast to WT and VGLUT3 heterozygous mice, which begin to show an ABR (ABR threshold) at ~35 dB SPL, VGLUT3 KO mice show no response over the range of intensities tested, indicating profound deafness (Figures 2B and 2C). We also tested the ABR at three different frequencies: 8, 16, and 32 kHz. Again, VGLUT3 KO mice show no response at up to 88.1 dB SPL (the highest intensity tested) for all three frequencies (Figure 2B).

The absence of evoked potentials under all conditions suggests that deafness in the VGLUT3 KO mice results from a peripheral defect in the cochlea or afferent neuronal pathway. We thus assessed mechanoelectrical transduction and the electromotility of outer hair cells (OHCs) by analyzing otoacoustic emission spectra (Figure 2D). VGLUT3 KO and heterozygous mice show no difference from WT littermates in otoacoustic emissions measured over a range of frequencies and at multiple intensities (Figure 2D and data not shown). This evidence for intact cochlear sound amplification, together with the lack of ABR evoked

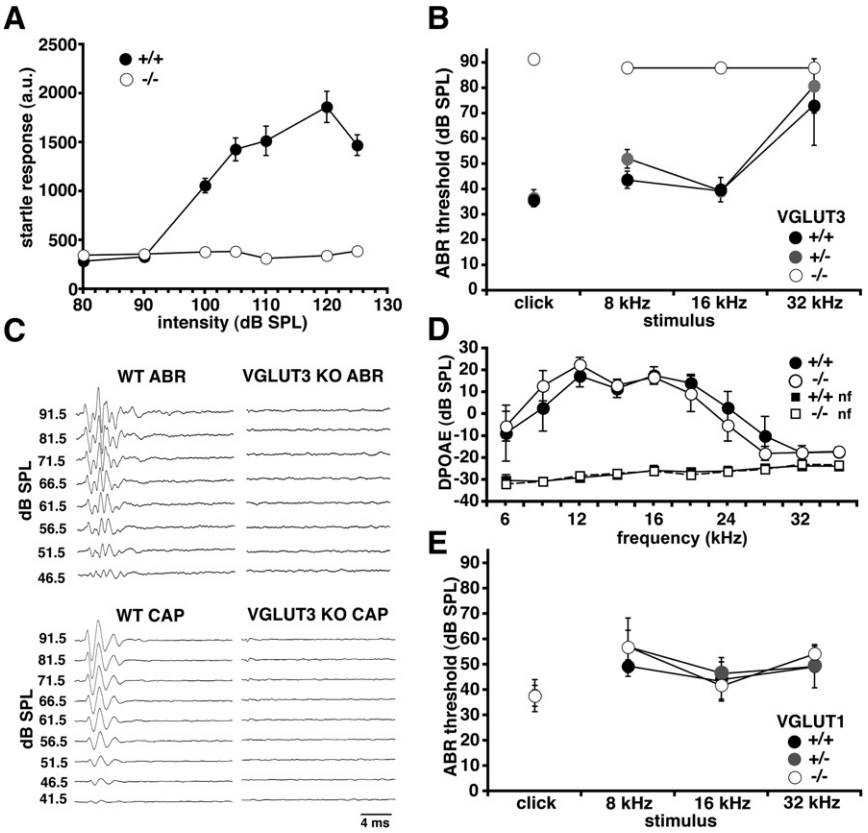

Figure 2. Sensorineural Deafness in VGLUT3 KO Mice

(A) Acoustic startle response of VGLUT3 KO mice (open circles, n = 7) and WT littermates (filled circles, n = 7) at sound intensities from 80 to 125 dB sound pressure level (SPL). KO mice show no response at any intensity.

(B) Auditory brainstem response (ABR) thresholds to click stimuli (up to 91.5 dB SPL) or pure tones (8, 16, and 32 kHz, at up to 88.1 dB SPL) for P21 WT (filled circles, n = 5), VGLUT3 heterozygotes (gray circles, n = 5), and VGLUT3 KO mice (open circles, n = 5). VGLUT3 KO mice show no response. Wild-type mice show an impairment at high frequency, consistent with impaired high-frequency hearing in the C57Bl/6 mice to which the VGLUT3 KO were backcrossed.

(C) Representative ABR (P21) and compound action potentials (CAP) (P14–17) for WT and VGLUT3 KO mice. A small stimulus artifact that precedes the onset of the CAP in WT mice is all that remains in the KO.

(D) Distortion product otoacoustic emissions spectra (DPOAE) measured at 65 dB SPL show no difference between WT (filled circles, n = 5), VGLUT3 heterozygotes (gray circles, n = 5), and VGLUT3 KO mice (open circles, n = 5). Nf is the noise floor measurement.

(E) ABR thresholds to click stimuli (up to 91.5 dB SPL) or pure tones (8, 16, and 32 kHz, at up to 88.1 dB SPL) for P21 WT (filled circles, n = 4) show no difference from VGLUT1 heterozygotes (gray circles, n = 5) and VGLUT1 KO mice (open circles, n = 4).

Error bars indicate the standard error of the mean.

potentials, indicates that a defect at the IHC-afferent synapse may underlie the deafness in VGLUT3 KO animals. To identify more precisely the location of the defect in sound-evoked potentials, we measured the auditory nerve compound action potential (CAP) elicited by sound (91.5 dB SPL), recording at the round window (Figure 2C). Under these conditions, we observed a large, complex waveform in P14–17 WT mice and no response in the KO (n = 4). The absence of even the earliest response to stimulation strongly suggests a defect in signaling between IHC and auditory nerve.

To determine whether an anatomical defect accounts for the deafness of VGLUT3 KO mice, we examined the morphology of the cochlea and spiral ganglion. By light microscopy, both inner and outer hair cells appear normal in P21 VGLUT3 KO mice (Figure 3A). By electron microscopy, P21 KO mice show abnormally thin, elongated ribbons in 26 out of 31 IHC synapses examined from three different KO animals. The morphology of synapses appeared normal in 5/31 IHC synapses from KO and 25/25 synapses from three WT mice (Figure 3B). However, the abnormality in synaptic ribbons seems unlikely to account for the deafness observed because bassoon knockout mice with almost no synaptically anchored ribbons exhibit a substantially milder hearing deficit (Khimich et al., 2005). We also counted the number of synaptic vesicles per section. WT mice show 12.7 ± 0.5 vesicles associated with ribbons (n = 18), and VGLUT3 KO mice show 12.8 ± 2.0 (n = 17). WT animals show 2.3 ± 0.6 vesicles morphologically docked at the plasma membrane, and VGLUT3 KO show 1.6 ± 0.6 ($p > 0.07$). The VGLUT3 KO thus does not differ significantly from WT in the number of synaptic vesicles tethered to ribbons or docked at the plasma membrane.

In the spiral ganglion, VGLUT3 KO mice exhibit a progressive loss of neurons at all levels of the cochlea (apex, mid-turn, base) that becomes readily apparent by P10 (Figure 3C, Table 1, and data not shown). Consistent with this, the cochlear nucleus, which contains projections from the spiral ganglion, shows a reduced volume (Figure 3D). However, this moderate neuronal loss also seems unlikely to account for the complete absence of CAPs observed in P14 KO mice (Figure 2C).

Inner Hair Cells Express VGLUT3

Immunofluorescence for all three VGLUT isoforms at P21 shows that IHCs label only for VGLUT3 (Figure 4A). Its distribution resembles that observed for other elements of the IHC release machinery, including the SNARE proteins VAMP1, SNAP-25, and syntaxin 1 that mediate vesicle fusion with the plasma membrane, and the putative calcium sensor otoferlin (Figure 4A) (Roux et al., 2006; Safieddine and Wenthold, 1999). We did not detect expression of VGLUT3 elsewhere in the organ of Corti. Sparse, punctate VGLUT1 and light VGLUT2 immunoreactivity surround inner and outer hair cells but do not colocalize with hair cell markers or the efferent synaptic vesicle protein synaptophysin (data not shown). To confirm the specificity of labeling, we

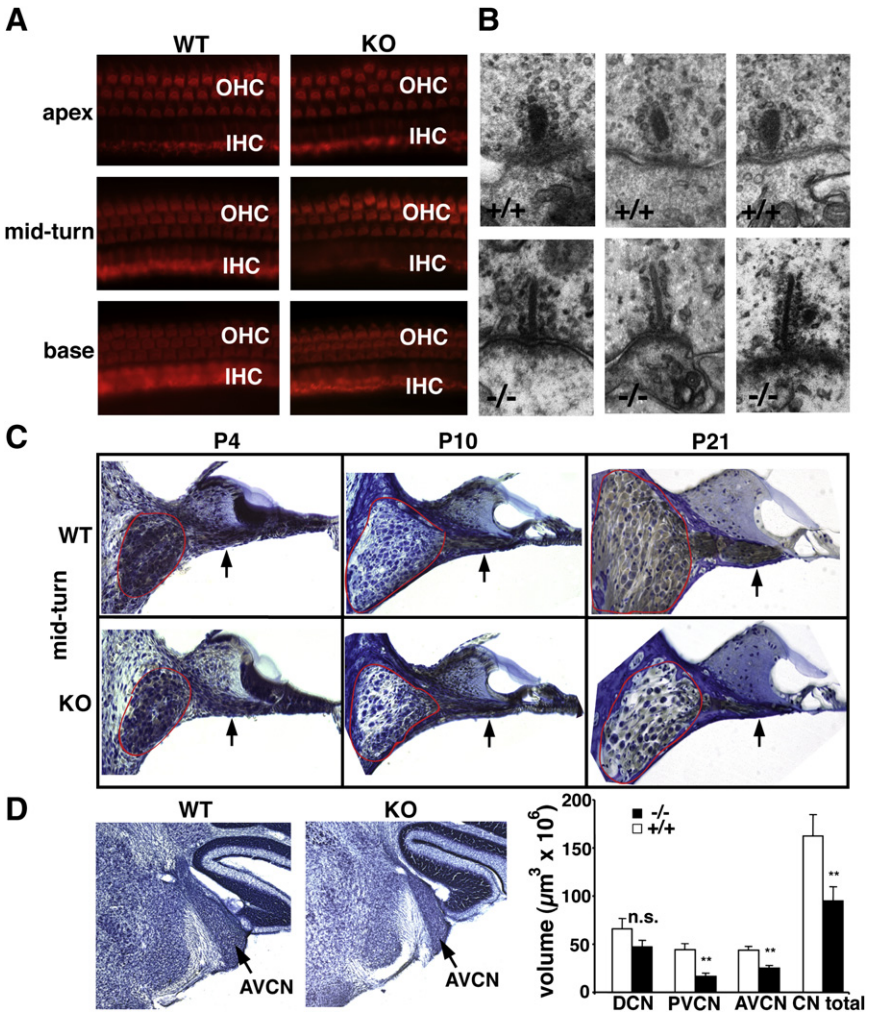

Figure 3. The Loss of VGLUT3 Affects Inner Hair Cell Ribbons and Spiral Ganglion Cell Survival

(A) Surface preparation of sensory hair cells from the apex, mid-turn, and base of P21 VGLUT3 KO mice shows no difference from WT by staining with rhodamine-phalloidin.

(B) Electron microscopy of inner hair cells (IHC) from P21 VGLUT3 KO (−/−) mice shows abnormally thin, elongated ribbons. IHC ribbon synapses from WT littermates (+/+) are shown for reference. 40,000× magnification.

(C) Sections from the mid-turn of WT and VGLUT3 KO cochlea at P4, P10, and P21 were stained with osmium tetroxide and toluidine blue. Spiral ganglia (outlined in red) from KO animals show fewer cells than WT at P10 and P21. The nerve fiber bundle (arrows) is also thinned in VGLUT3 KO mice.

(D) Volume of the posteroventral cochlear nucleus (PVCN) and AVCN but not dorsal cochlear nucleus (DCN) is significantly reduced in VGLUT3 KO mice. ($n = 4$, $p < 0.01$, Student's t test.)

Error bars indicate standard error of the mean.

immunostained the cochlea of VGLUT3 KO mice and detected no immunoreactivity for VGLUT3 (Figure 4A). In addition, the IHCs of VGLUT3 KO mice show no upregulation of VGLUT1 or -2 (data not shown).

The VGLUTs undergo developmental regulation in other parts of the nervous system (Boulland et al., 2004; Fremeau et al., 2004a; Gras et al., 2005; Miyazaki et al., 2003), raising the possibility that their transient expression at a critical time in development might exert a long-term effect on hearing. We thus examined the time course of VGLUT expression in the cochlea. At E15, IHCs do not express any of the VGLUTs. However, by E19 and at all subsequent ages tested, the IHCs express VGLUT3 (Figure 4B). Around the time of birth, OHCs labeled weakly for VGLUT3 (Figure 4B), but VGLUT1 and -2 were not detected in inner or outer hair cells at any age (Figure 4A and data not shown). The sole expression of VGLUT3 by IHCs throughout development and maturity suggests that the degeneration observed in KO mice results directly from an impairment in glutamate release.

To assess further VGLUT expression by IHCs, we have used RT-PCR. In IHCs (obtained from rat due to the more precise dissection), we detect only mRNA for VGLUT3 and the nicotinic receptor subunit (nAChR) α9 (Figure 4C), a gene expressed in the cochlea exclusively by hair cells. We do not detect transcripts for VGLUT1 or -2. In contrast, the cochlea as a whole expresses all three VGLUT isoforms as well as the α9 nAChR subunit (Figure 4C). No VGLUT or α9 nAChR transcripts were detectable by RT-PCR from the dissection medium (data not shown). Thus, IHCs express only the VGLUT3 isoform.

Since previous work has suggested the expression of VGLUT1 by IHCs (Furness and Lawton, 2003), we also examined hearing in the VGLUT1 KO mice (Fremeau et al., 2004a). VGLUT1 KO mice exhibit a robust startle to loud clap, and ABR thresholds to click and pure tone stimuli do not differ from WT littermates (Figure 2E). Otoacoustic emission spectra of VGLUT1 KO mice are also normal (data not shown).

Table 1. Density of Spiral Ganglion Neurons in WT and VGLUT3 KO Mice

	P10		P21	
	WT	KO	WT	KO
Apex	1056 ± 76	812 ± 68*	800 ± 63	517 ± 20***
Mid-turn	1042 ± 88	804 ± 42*	799 ± 25	486 ± 21***
Base	867 ± 16	536 ± 9**	709 ± 64	374 ± 10***

Spiral ganglion densities (cells/mm^2) at the apex, mid-turn, and base were calculated for VGLUT3 KO and WT mice at P10 and P21. Values indicate mean ± standard deviation, and significance was determined by Student's t test, with $p < 0.05$ denoted by *, $p < 0.01$ by **, and $p < 0.005$ by ***.

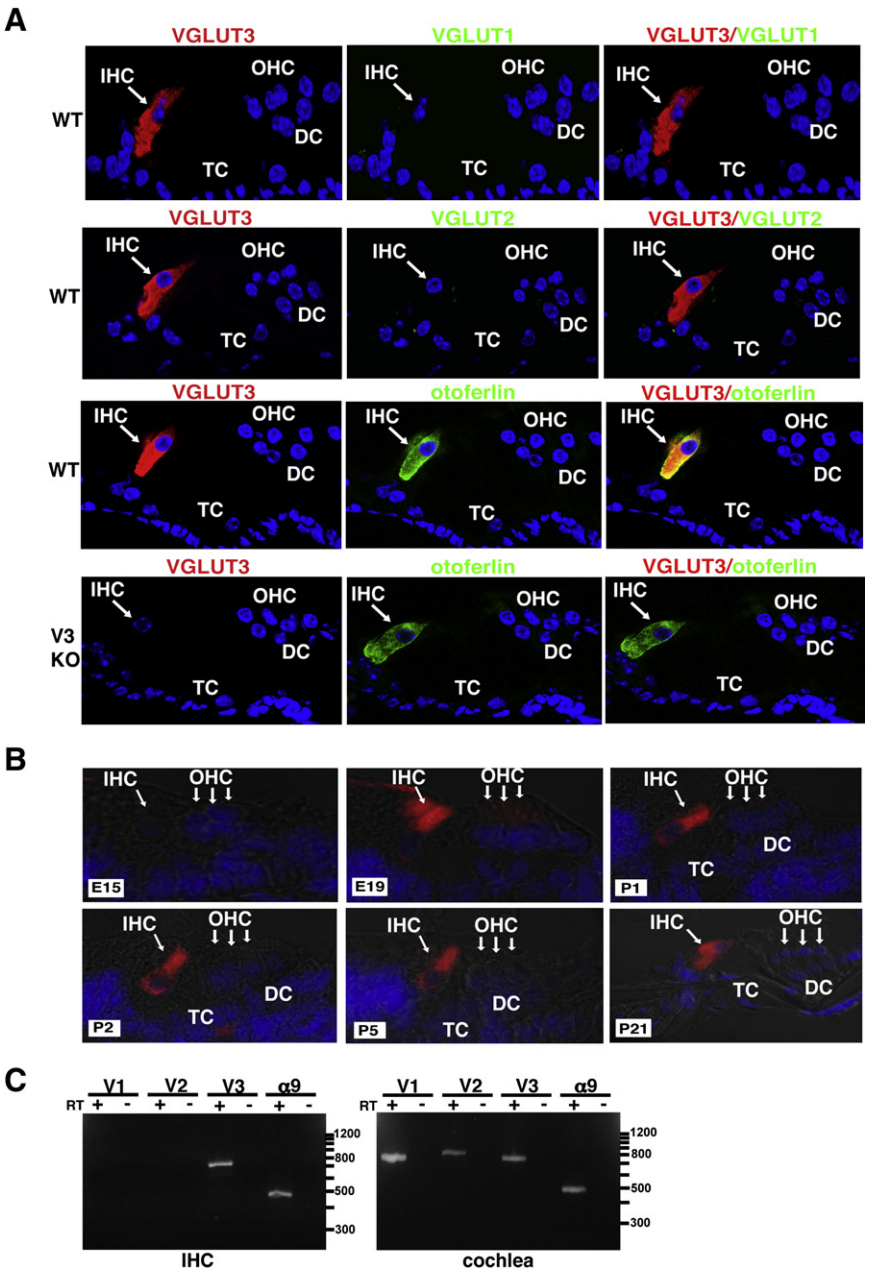

Figure 4. VGLUT Expression in the Organ of Corti

(A) Immunofluorescence for VGLUT3 (red) and either VGLUT1 (green) or VGLUT2 (green) in cochlea of P21 WT mice shows expression of only VGLUT3 by IHCs. VGLUT3 immunoreactivity (red) localizes to the IHC in a pattern resembling that of the synaptic vesicle protein otoferlin (green). P21 VGLUT3 KO mice show no immunoreactivity for VGLUT3 (red), while otoferlin expression appears normal (green). Nuclei are stained with DAPI (blue).

(B) VGLUT3 (red) becomes detectable by immunofluorescence in the cochlea of WT mice by E19. OHC, outer hair cell; TC, Tunnel of Corti; DC, Deiters cells.

(C) RT-PCR of P13–14 rat IHCs shows expression of only the VGLUT3 isoform and the nAChR subunit α9, a gene expressed exclusively by hair cells within the cochlea. The cochlea as a whole expresses all three VGLUT isoforms and the nAChR α9. No products were detected when RT-PCR was performed in the absence of reverse transcriptase (−RT).

VGLUT3 KO Mice Exhibit Developmentally Regulated IHC Conductances Similar to Wild-Type

Morphological abnormalities in the cochlea of VGLUT3 KO mice raise the possibility that the defect in synaptic transmission results secondarily from changes in the properties of IHCs or ganglion cells rather than a primary defect in transmitter release. We have therefore examined several key conductances expressed by IHCs and tested the developmental regulation for some of them. In hair cells, voltage-gated L-type calcium channels mediate the calcium influx required to trigger neurotransmitter release. Recording at the end of the first postnatal week when these currents reach a transient maximum (Johnson et al., 2005; Moser and Beutner, 2000), VGLUT3 KO and wild-type mice both exhibit a bell-shaped current-voltage relationship with activation at ~−64 mV and peak current at ~−14 mV (Figures 5A and 5B). Current amplitudes were not significantly different between VGLUT3 KO and WT mice over the whole voltage range ($p = 0.7$). The rates of activation by depolarization to −14 mV were also similar, with time constants of 0.32 ± 0.04 ms for VGLUT3 KO mice and 0.31 ± 0.03 ms for WT ($p = 0.2$). All these features of IHC calcium channels are very similar to previous reports (Brandt et al., 2007; Johnson et al., 2005; Moser and Beutner, 2000; Platzer et al., 2000; Sendin et al., 2007).

IHCs fire calcium action potentials before the onset of hearing (Kros et al., 1998; Marcotti et al., 2003), and calcium action potentials were observed spontaneously in 7 out of 10 VGLUT3 KO mice at P7–8 and in 7 out of 9 WT animals. Current injection induced calcium action potentials in 5 of 5 KO and 6 of 6 WT (Figure 5C). After the onset of hearing, however, current injection did not induce calcium action potentials in the IHCs of either KO (3 of 3) or WT (8 of 8) mice (Figure 5D). This loss of excitability is thought to result in part from the appearance of BK potassium channels, which short-circuit the generation of calcium action potentials (Kros et al., 1998).

IHCs express multiple developmentally regulated potassium conductances (Kros et al., 1998; Marcotti et al., 2003; Pyott et al., 2004). Before hearing, IHCs exhibit slowly activating delayed rectifier potassium currents. After hearing onset, a rapidly activating large conductance calcium-dependent BK current also appears. Very similar to WT animals, the IHCs of VGLUT3 KO mice show an ~20-fold slower activation time constant at

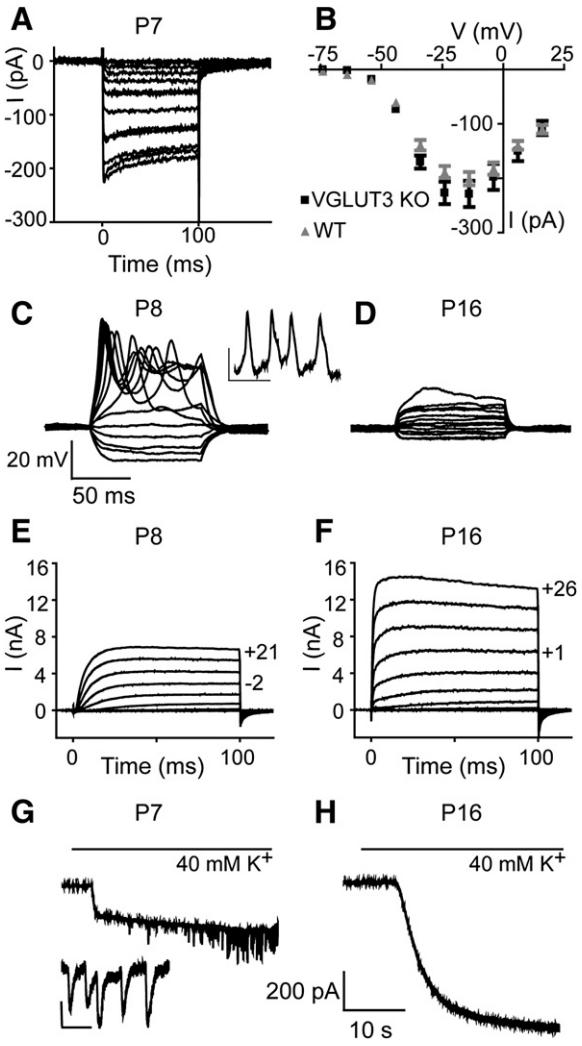

Figure 5. VGLUT3 KO Mice Exhibit Developmentally Regulated Inner Hair Cell Conductances Similar to WT

(A) IHC calcium currents recorded from a P7 VGLUT3 KO mouse in response to 100 ms depolarizations from −84 mV to +16 mV in 10 mV increments.

(B) Similar current-voltage relationships for calcium currents from P7–8 VGLUT3 KO (n = 9) and WT IHCs (n = 9). Current amplitudes were measured after full activation, and the values presented are mean ± SE.

(C) Calcium action potentials produced by current injection into a P8 VGLUT3 KO IHC. 100 ms current steps were applied from −40 pA in 10 pA increments. In this cell, calcium action potentials were generated with +20 pA current injection. Inset shows spontaneous calcium action potentials recorded from a VGLUT3 KO IHC in the absence of current injection. Scale: 20 mV and 200 ms.

(D) Using the same protocol, a P16 VGLUT3 KO IHC shows no calcium action potentials.

(E and F) Potassium currents recorded from P8 (E) and P16 (F) VGLUT3 KO IHCs in response to 100 ms voltage steps from −104 mV to +26 mV in 10 mV increments from a holding potential of −84 mV (nominal voltages). Actual voltages reached after correcting for series resistance error are shown next to selected traces.

(G) Depolarization with 40 mM extracellular potassium activates synaptic currents from cholinergic efferents in a VGLUT3 KO IHC at P7. Inset shows single synaptic currents on an expanded timescale (30 pA, 250 ms).

(H) No synaptic currents are detected in a VGLUT3 KO IHC at P16. The slow rise in inward current in both (G) and (H) results from the change in K^+ equilibrium potential produced by addition of 40 mM K^+.

Error bars indicate standard error of the mean.

P8, before hearing, than at P15–16, after hearing onset ($p < 0.01$) (Figures 5E and 5F and Table 2). In addition, the amplitude of outward currents increases 2- to 3-fold from P8 to P15–16 in both KO and WT mice ($p < 0.01$) (Figures 5E and 5F and Table 2). At both ages, there was no difference between the activation time constant of KO and WT ($p > 0.5$). However, current amplitudes are slightly larger for VGLUT3 KO mice ($p < 0.01$) (see Figure S1 available online). Nonetheless, potassium conductances undergo very similar developmental regulation in both VGLUT3 KO and WT animals.

Before the onset of hearing at P12–14, IHCs receive cholinergic inputs that disappear in the third postnatal week (Katz et al., 2004; Simmons et al., 1996; Simmons, 2002). At P7–8, depolarization of efferents with 40 mM K^+ produced synaptic currents in all the IHCs tested from both VGLUT3 KO (8 of 8) and WT (7 of 7) mice (Figure 5G). In contrast, at P15–16, only a small proportion of IHCs responded (1 of 9 KO and 1 of 8 WT mice) (Figure 5H). The loss of VGLUT3 thus does not appear to influence the developmental change in innervation by IHC efferents.

Loss of VGLUT3 Eliminates Synaptic Glutamate Release from IHCs

To assess directly neurotransmission at the first synapse in the auditory pathway of VGLUT3 KO mice, we performed whole-cell recordings from auditory nerve fiber terminals at the site where they contact the IHC (Glowatzki and Fuchs, 2002). The current-voltage relationship of afferents from VGLUT3 KO mice showed features typical of recordings from WT terminals (Figures 6A and 6B), with a fast sodium current, low voltage activating and high voltage activating potassium conductances, and occasional I_h current (E.Y. and E.G., unpublished data). Depolarizing with 20–40 mM K^+ to induce synaptic activity, all recordings from WT mice (n = 10) showed synaptic currents reversibly blocked by the AMPA receptor antagonist NBQX (10 μM) (Figure 6C). Spontaneous synaptic currents were also observed at low frequency (<1 Hz) in WT recordings (7 of 10). However, no synaptic response was detected in KO mice (n = 11), even with depolarization by elevated K^+ (Figure 6D). To determine whether the absence of synaptic response might be due to the loss of glutamate receptors, we applied 10–100 μM kainic acid (KA) along with 100 μM cyclothiazide to prevent receptor desensitization. At a holding potential of −94 mV, kainate induced inward currents in both WT (5 of 5) and VGLUT3 KO (4 of 4) animals (Figures 6E and 6F). The kainate-induced currents were blocked by NBQX, indicating their dependence on AMPA receptors. The afferents of VGLUT3 KO mice thus exhibit a normal response to direct receptor stimulation, indicating that the defect in neurotransmission must be presynaptic, due to a loss of glutamate release.

Nonconvulsive Seizures in VGLUT3 KO Mice

The importance of VGLUT3 for glutamate release by IHCs suggests that the transporter may also contribute to signaling at synapses usually associated with a different transmitter. Indeed,

Table 2. Properties of Inner Hair Cell Potassium Conductances at P8 and P15–16 for WT and VGLUT3 KO Mice

	WT			KO		
Age	τ_{act} (ms)	amplitude (nA)	n	τ_{act} (ms)	amplitude (nA)	n
P8	9.6 ± 1.0	3.9 ± 0.3	6	7.4 ± 0.8	5.7 ± 0.6	6
P15–16	0.47 ± 0.1	6.9 ± 0.6	6	0.37 ± 0.1	15.9 ± 1.5	8

Current amplitudes elicited by depolarization to +4 mV, measured at the end of 100 ms voltage steps. Values are presented as mean ± SE. For both VGLUT3 KO and WT mice, current amplitudes change significantly with age ($p < 0.01$). For P15/16 IHCs, potassium current amplitudes in VGLUT3 KO mice were significantly larger than in WT ($p < 0.01$).

VGLUT3 is expressed by a subset of GABAergic basket cells in the hippocampus and cortex, suggesting that these neurons release glutamate as well as GABA (Hioki et al., 2004; Somogyi et al., 2004). Since signaling by interneurons is known to influence network activity, we monitored 3- to 7-month-old KO animals for extended periods by combined electroencephalography (EEG) and digital video. The background cortical activity in all VGLUT3 KO mice shows frequent (5–10/min) generalized synchronous discharges that were never observed in WT littermates (Figure 7A). The high-amplitude discharges are of two distinct types, a broad surface-negative spike and sharp wave complex lasting 200–300 ms and occasional inverted positive sharp spikes, neither of which was accompanied by myoclonic behavior. This baseline activity demonstrates a neocortical hyperexcitability usually associated with convulsive seizures in mouse models and in humans. Indeed, EEG recording shows that the VGLUT3 KO animals have intermittent, spontaneous cortical seizures lasting up to 2 min. However, the mice exhibit remarkably little behavioral accompaniment throughout the entire electrographic seizure and remain either immobile with no associated myoclonic activity or display normal exploratory behavior (Movies S1 and S2). At seizure onset, the EEG shows generalized or occasionally unilateral onset of fast spike and slow wave activity, followed by continuous spike discharges decelerating to a slow (1–3/s) spike-wave rhythm (Figure 7B). The episodes conclude with a pattern of alternating accelerated spikes and spike-wave activity and terminate abruptly by returning to pre-ictal patterns, with no EEG flattening (Figure 7B and Movies S1 and S2). These nonconvulsive electrographic seizures occur once per day on average, and no generalized tonic-clonic motor activity was observed despite prolonged monitoring. Interestingly, mice heterozygous for the VGLUT3 null allele also show interictal epileptiform abnormalities, but no detectable electrographic seizures (Figure 7A).

DISCUSSION

The results show that VGLUT3 serves as an important mediator of glutamate signaling, with essential roles in the auditory system and cortex. VGLUT3 KO mice are entirely deaf, and the loss of auditory brainstem responses indicates a defect early in the auditory pathway, within the cochlea. Intact otoacoustic emissions exclude a problem with mechanoelectrical transduction or outer hair cell motility. Rather, the analysis of compound action potentials recorded from the auditory nerve suggests impairment of neurotransmission at the IHC-afferent synapse. However, the

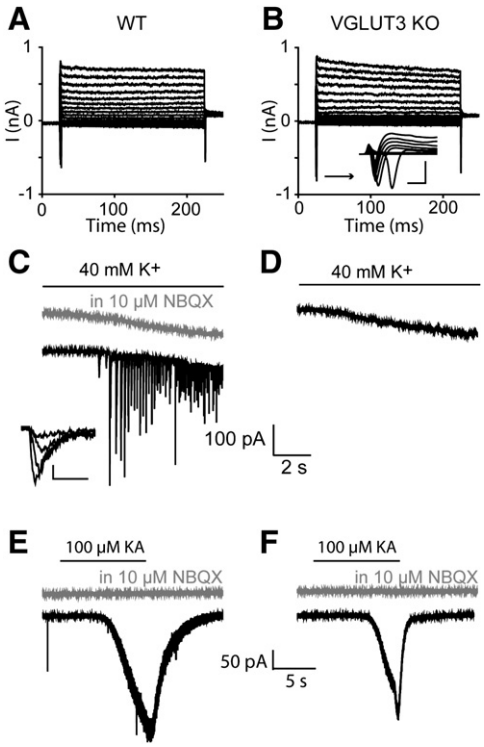

Figure 6. Absence of Synaptic Activity in the Afferent Terminals of VGLUT3 KO Mice

(A and B) I-V relationships recorded from IHC afferent terminals in response to 200 ms voltage steps from −104 to +36 mV in 10 mV increments (holding potential −84 mV) show no difference between WT (A) and VGLUT3 KO mice (B). Inset in (B) shows Na^+ currents on an expanded timescale for voltage steps from −84 to −4 mV (0.5 nA, 1 ms).

(C and D) Afferent terminal responses to depolarization with 40 mM potassium (holding potential −94 mV) show AMPA receptor-mediated synaptic currents completely blocked by 10 μM NBQX in WT animals (C). Inset shows individual synaptic currents on an expanded timescale (50 pA, 2 ms). (D) No synaptic activity was detected in the afferent terminals of VGLUT3 KO mice. The slow rise in inward current in (C) and (D) reflects the change in K^+ equilibrium potential due to addition of 40 mM K^+.

(E and F) 100 μM kainate (KA) (with 100 μM CTZ to prevent AMPA receptor desensitization) evokes inward currents in both WT (E) and VGLUT3 KO (F) afferent terminals (holding potential −94 mV). Kainate-evoked currents were completely blocked by 10 μM NBQX.

IHCs of VGLUT3 KO mice exhibit physiological properties very similar to WT animals. In particular, the IHCs of VGLUT3 KO mice show normal calcium currents, and at hearing onset, the normal downregulation of calcium action potentials together with the appearance of BK potassium conductances, a process that appears to depend on thyroid hormone (Brandt et al., 2007; Rusch et al., 2001; Sendin et al., 2007). Afferent nerve terminals of KO mice also exhibit sodium and potassium conductances very similar to WT. However, KO afferents lack synaptically evoked glutamate receptor currents despite normal responses to exogenous kainate, indicating a specific, presynaptic defect in glutamate release. Glutamate has been proposed as the primary transmitter at the IHC-afferent nerve synapse (Bobbin, 1979; Comis and Leng, 1979; Ottersen et al., 1998). Since the only VGLUT isoform expressed by IHCs is VGLUT3,

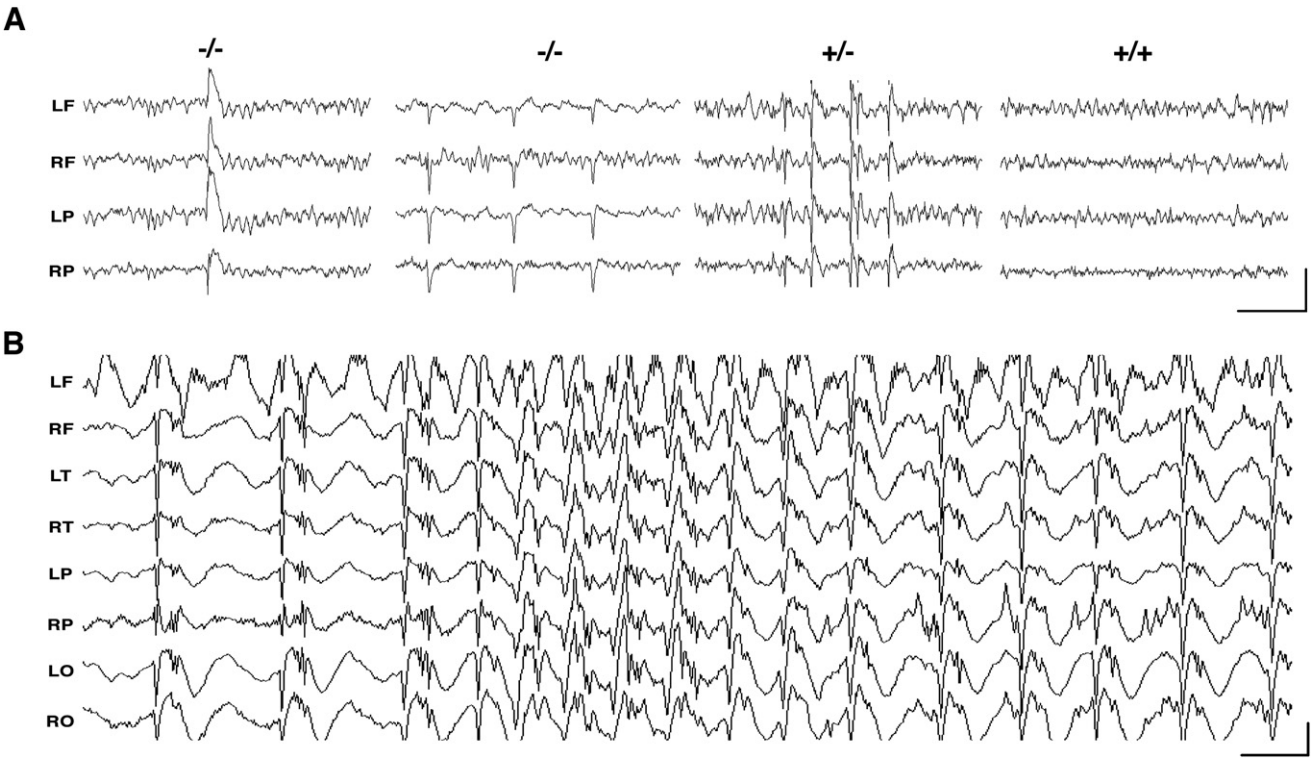

Figure 7. VGLUT3 KO Mice Exhibit Seizures and Frequent Interictal Spike Discharges

(A) Chronic EEG recording shows two distinct types of interictal discharge in VGLUT3 KO mice (−/−), one a long-lasting spike-wave complex and the other a positive-going sharp spike discharge. Mice heterozygous for VGLUT3 (+/−) also show sharp interictal spike discharges, but no discharges or baseline EEG abnormalities were recorded from wild-type (+/+) littermates.

(B) VGLUT3 KO mice show prolonged generalized spike-wave seizure discharges with no apparent effects on motor behavior (Movies S1 and S2). All leads are recorded using a digital average reference source. Calibration bars: (A) 1.25 s, 500 μV, (B) 1 s, 500 μV. Electrode montage: LF, left frontal; RF, right frontal; T, temporal; P, parietal; O, occipital.

the absence of glutamate release in KO mice must reflect a loss of vesicle filling. IHCs have been reported to express VGLUT1 (Furness and Lawton, 2003), but we could not detect specific expression of either VGLUT1 mRNA or protein by IHCs, and the VGLUT1 KO shows no measurable hearing impairment. The loss of VGLUT1 or indeed other vesicular neurotransmitter transporters does not obviously impair synaptic vesicle exo- or endocytosis (Croft et al., 2005; Wojcik et al., 2004), making it unlikely that the loss of VGLUT3 would affect these other aspects of the synaptic vesicle cycle.

VGLUT3 belongs to a small number of proteins involved in neurotransmitter release that have a relatively selective effect on synaptic signaling by IHCs. Otoferlin, a protein associated with hereditary deafness in humans (Yasunaga et al., 1999), has recently been suggested to act as the principal calcium sensor for regulated exocytosis in mammalian IHCs (Roux et al., 2006). Deletion of the otoferlin gene in mice results in profound deafness due to the loss of synchronous evoked glutamate release at the IHC-afferent synapse. Similar to the VGLUT3 KO, the IHCs of otoferlin KO mice show relatively normal ionic conductances. However, both otoferlin and VGLUT3 KO mice show an increase in IHC K^+ currents at maturity, suggesting feedback of the glutamate signal onto IHCs. In contrast, mice lacking the calcium channels required for transmitter release do not exhibit the usual appearance of BK potassium currents and loss of efferents seen in both VGLUT3 KO, otoferlin KO, and WT animals (Brandt et al., 2003; Nemzou et al., 2006), indicating that these changes do not rely on synaptic transmission but rather on the specific activity of calcium channels.

The loss of VGLUT3 produces morphological changes in the cochlea similar to those previously observed in otoferlin KO animals (Roux et al., 2006). VGLUT3 KO mice show a progressive reduction in the number of ganglion cells during postnatal development, as well as their projections to the brainstem. Indeed, stimulation (presumably mediated by glutamate) has been shown to provide trophic support for spiral ganglion cells (Hegarty et al., 1997). The IHCs of both otoferlin and VGLUT3 KO mice also show abnormal ribbons, although the ribbons in otoferlin KO have defects in anchoring to the synaptic membrane, and those in VGLUT3 KO exhibit an abnormally elongated morphology. However, the number of synaptic vesicles, their association with ribbons, and their morphological docking at the plasma membrane appear unaffected by the loss of VGLUT3.

The appearance of VGLUT3 before birth provides a mechanism for neurotransmission before the onset of hearing, as previously shown (Eybalin et al., 2004; Glowatzki and Fuchs, 2002; Knipper et al., 1997). Since spontaneous retinal activity influences development of the visual system (Eglen et al., 2003; Firth et al., 2005;

Shatz, 1996), the early expression of VGLUT3 by IHCs may therefore also contribute to development of the auditory system. Indeed, the transient expression of VGLUT3 at the synapse made by medial nucleus of the trapezoid body neurons onto lateral superior olivary neurons (MNTB-LSO synapse) has suggested an early role for activity in tonotopic refinement and synaptic strengthening downstream in the pathway (Gillespie et al., 2005). Consistent with previous work, the degenerative changes observed at P10 in VGLUT3 KO mice demonstrate that early activity has a specific role in development of the auditory system.

Similar to IHCs, retinal photoreceptors and bipolar cells form ribbon synapses, but express VGLUT1 (Johnson et al., 2003; Sherry et al., 2003). How might the properties of the unconventional isoform VGLUT3 help to fulfill the specialized function of the IHC synapse in hearing? Although the isoforms differ little in their intrinsic transport activity, they diverge substantially in trafficking (Voglmaier et al., 2006). The dendritic targeting of VGLUT3 in multiple neuronal populations (Fremeau et al., 2002; Harkany et al., 2004) may indeed correspond to its basolateral targeting in epithelial cells such as IHCs. In addition, IHCs appear to derive their synaptic vesicles from at least two sources: one a local recycling pool at the basolateral surface that involves cisternal intermediates (Lenzi et al., 2002), and another pool particularly important for sustained, high-frequency synaptic signaling that may originate on the apical surface (Griesinger et al., 2002, 2005). The neuronal localization of VGLUT3 in dendrites as well as axons is indeed consistent with its trafficking to more than one pool of secretory vesicles.

The incessant interictal activity and less frequent generalized seizures observed in VGLUT3 KO mice indicate a major disturbance of cortical excitability. A distinguishing feature of these seizures is the lack of overt changes in ongoing motor behavior. Absence epilepsy in human patients and animal models involves brief (1–10 s), highly stereotyped thalamocortical discharges, but these episodes are always accompanied by behavioral arrest and often terminate with myoclonus (Noebels and Sidman, 1979). In contrast, VGLUT3 KO mice provide the first genetically defined mouse model of pure primary generalized nonconvulsive epilepsy demonstrating essentially complete electrographic dissociation, with no prominent effects on behavior. The loss of VGLUT3 appears sufficient to synchronize a limited cellular network without allowing spread to pathways mediating tonic or clonic motor activity, providing an entry point to identify the anatomic substrate for dissociated cortical hypersynchrony.

It is interesting that the loss of one VGLUT3 allele confers interictal epileptiform abnormalities without evident electrographic seizures. VGLUT1 and -2 heterozygotes have no obvious behavioral phenotype, but a recent study of the VGLUT1 heterozygote has suggested abnormalities in anxiety and long-term memory (Tordera et al., 2007). The VGLUT2 heterozygote shows a specific defect in nociception (Moechars et al., 2006). Although apparently sufficient to fill vesicles under baseline conditions even when substantially reduced (Daniels et al., 2006), VGLUT expression may thus become limiting under certain conditions, possibly related to increases in activity. The interictal abnormalities observed in VGLUT3 heterozygous mice may reflect a similar requirement for two wild-type alleles, with one sufficient to prevent the development of generalized seizures. Considering the extreme demands of signaling by IHCs, it is notable that VGLUT3 heterozygotes exhibit no obvious hearing impairment, but future study may reveal more subtle abnormalities in sound processing.

The importance of VGLUT3 for neurotransmission at the IHC synapse known to use glutamate suggests that the transporter also contributes to glutamate release by neurons usually associated with a different transmitter. Indeed, VGLUT3 in the cortex localizes primarily to GABAergic interneurons, as well as to serotonergic projections from the raphe nuclei (Hioki et al., 2004; Somogyi et al., 2004). Interestingly, dysfunction in a subset of cortical and hippocampal interneurons due to loss of the DLX1 transcription factor produces seizures resembling those observed in VGLUT3 KO animals (Cobos et al., 2005), suggesting that the VGLUT3 KO seizure phenotype reflects the loss of glutamate signaling by inhibitory interneurons. VGLUT3 thus has a physiologically important role in the control of cortical excitability, presumably by conferring the release of glutamate from cells usually associated with GABA. These observations strongly suggest that VGLUT3 also contributes to glutamate signaling by neurons traditionally considered to release other transmitters.

EXPERIMENTAL PROCEDURES

Generation of VGLUT3 Knockout Mice

A bacterial artificial chromosome (BAC) containing the *vglut3* genomic locus from mouse strain 129S6/SvEvTac was used as a template for PCR to amplify a 4.5 kb fragment encompassing part of the third intron (right arm) with primers 5′-cagagccattcattgattgatgtaag-3′ and 5′-catcacctgaccctactgagtaataa-3′. The product was subcloned into pPNT (Tybulewicz et al., 1991) at BamHI and KpnI sites 3′ to the neomycin cassette. pPNT was modified to include loxP sites surrounding the neomycin cassette. A 2.4 kb fragment (left arm) encompassing part of the second intron and the first 35 base pairs of the second exon was amplified by PCR using 5′-ctgactctgtggtctcaaagtgctag-3′ and 5′-tggtcccatcgattttcttcatcacc-3′ and subcloned at NotI and XhoI sites 5′ to the neomycin cassette. The gene encoding the enhanced version of green fluorescent protein (EGFP) including the stop codon and polyadenylation site was inserted into the XhoI site of pPNT. The resulting construct was linearized by digestion with Not1 and transfected into 129/Ola embryonic stem cells (UCSF Transgenic Core) (Soriano et al., 1991; Thomas and Capecchi, 1987). ES cell clones resistant to both neomycin and gancyclovir were analyzed by Southern blotting of BamH1-digested DNA with the 5′ probe shown in Figure 1A. Out of 300 colonies screened, two had undergone homologous recombination, and each was injected into mouse blastocysts to generate chimeric male mice, which were then mated to C57Bl/6 females. Chimeras from only one of the clones (11-3; Figure 1C) showed germ-line transmission of the recombined allele. Heterozygotes from this line were mated to each other and also backcrossed to C57Bl/6 animals. Although the gene coding for EGFP was inserted in-frame with the N-terminal protein-coding sequence of VGLUT3, EGFP was not observed by immunofluorescence in VGLUT3 KO brain slices. To eliminate possible interference by the positive selectable marker, we excised the neomycin cassette by crossing the F2 VGLUT3 heterozyous mice to mice expressing cre recombinase under the control of the β-actin promoter (which confers expression in the germline), but still failed to detect EGFP expression. Genotyping was carried out by PCR using a set of primers that only recognizes the wild-type allele (WT sense: 5′-gaaggaaggcccgtgcagac-3′ and WT antisense: 5′-cttatgtccctaacacatcatg-3′) and a set of primers that only recognizes the recombined allele (KO sense: 5′-caatgacgataatgatgatagtaac-3′ and KO antisense: 5′-gacacgctg aacttgtggccgtttac-3′.

Western Blotting

Crude membrane extracts including synaptic vesicles were prepared from brains of VGLUT3 KO mice and WT littermates, as described previously (Fon et al., 1997). Briefly, the brains were homogenized in 1 ml SH buffer (0.32 M

sucrose/10 mM HEPES, pH 7.4) with ten strokes at 900 rpm, sedimented at 1000 × g for 10 min, and the resulting supernatant at 200,000 × g for 60 min. Each sample (10 μg) was separated by electrophoresis through 10% SDS-polyacrylamide, transferred to immobilon, and probed with guinea pig (GP) anti-VGLUT3 (1:10,000) and mouse anti-synaptophysin (1:3000; Sigma) followed by incubation with goat anti-GP (1:10,000) or to goat anti-mouse (1:3000) (Jackson ImmunoResearch) conjugated to horseradish peroxidase and detection by enhanced chemiluminescence (Amersham Biosciences) using double emulsion film (Kodak BioMax XAR).

Light and Electron Microscopy

For brain slices, adult mice were anesthetized with nembutal and transcardially perfused with 4% paraformaldehyde (PFA) in phosphate-buffered saline, pH 7.4 (PBS), the brains removed, postfixed in 4% PFA, and transferred to 30% sucrose. Cryostat sections were incubated as previously described (Fremeau et al., 2001) with GP anti-VGLUT3 (1:10,000) and either rabbit anti-VAChT (1:1000), rabbit anti-VGLUT1 (1:1000), or rabbit anti-VGLUT2 (1:1000) at 4°C overnight, followed by incubation with donkey anti-GP antibody conjugated to Cy3 (1:2000) and donkey anti-rabbit antibody conjugated to FITC (1:1000). The sections were mounted using Prolong Antifade Gold (Molecular Probes/Invitrogen) and examined by confocal laser microscopy. Nissl stain was performed using NeuroTrace 500/525 (InVitrogen).

Sections of cochlea from WT (E15, E19, P1, P2, P5, P21) and VGLUT3 KO (P21) were prepared as previously described (Akil et al., 2006), preincubated for 1 hr in PBS containing 0.25% Triton X-100 and 5% normal goat serum (incubation buffer), and then incubated overnight at 4°C with primary antibodies: GP anti-VGLUT1 (1:5000; Chemicon), GP anti-VGLUT2 (1:2500; Chemicon), rabbit anti-otoferlin (gift from C. Petit), GP anti-VGLUT3 (1:10,000), or rabbit anti-VGLUT3 (1:500; Synaptic Systems, respectively). Sections were then washed and incubated for 2 hr with goat anti-rabbit IgG conjugated to FITC (1:2000), goat anti-GP IgG conjugated to Cy3 (1:2000). The sections were rinsed in PBS, incubated with DAPI (1.5 μg/ml in PBS; Sigma, St. Louis, MO) to counterstain nuclei, mounted in glycerol/PBS (1:1 v:v) or in Prolong Antifade Gold (Invitrogen/Molecular Probes), and examined by confocal microscopy.

Cochlear nucleus volume was measured in P14–15 mice anesthetized with Isovet and perfused with PBS containing 4% PFA and 1% glutaraldehyde. After incubation in 30% sucrose, sections were cut at 50 μm, mounted, stained with thionine, and the boundaries of cochlear subnuclei traced using Neurolucida version 6.0 (Microbrightfield, Inc.) The Cavalieri method was used for 3D reconstruction and volume calculations. Statistical analysis was performed using the two-tailed Student's t test.

Examination of hair cells and histopathology were performed as previously described (Akil et al., 2006). Spiral ganglion cell counts were performed on P10 and P21 mice (3 WT and 3 KO at each age). Cochleae were fixed as previously described (Akil et al., 2006). Serial 5 μm sections were cut parallel to the modiolus, stained with Toluidine Blue, and mounted with Permount. Eight serial mid-modiolar sections were selected from the apex, mid-turn, and base of each cochlea with approximately the same orientation relative to the mid-modiolus. In each section, the area of Rosenthal's canal was determined using a calibrated cursor (Image J). Cell counts from each section were based only on cells with visible nucleoli and were corrected for redundancy using the method of Abercrombie (Abercrombie, 1946). Cell densities from the eight sections were averaged, and the reported cell densities values for each condition are the mean and standard deviation from three mice. Data were collected blind to the genotype, and statistical analysis was performed using the Student's t test.

Electron microscopy was performed as previously described (Akil et al., 2006) except that serial sections through the synaptic region of inner hair cells were cut in a horizontal plane parallel to the basilar membrane. The morphological assessment of ribbons and vesicles was done using 15 to 16 different IHCs from three WT and three KO mice.

RT- PCR of IHC and Cochlea

IHCs from P13–14 rats were dissected away from the rest of the cochlea, pooled, and both IHCs and whole cochlea used as template for reverse transcriptase (RT)-PCR, as previously described (Akil et al., 2006), using SuperScript II RNase H- (Invitrogen) and oligo-dT primer for 50 min at 42°C. Reactions without the reverse transcriptase enzyme (−RT) were performed as control, and reactions using the dissection medium as template were used to control for contamination from lysed cells. The +RT (and −RT control) reaction products (2 μl) were then added to individual PCR reactions (*GoTaq* polymerase; Promega), each containing a set of intron-spanning primers designed to amplify specifically individual VGLUT isoforms, as well as the nAChR α9 subunit. Primer sequences are as follows: VGLUT1 forward (ctttctacctgctcctcatctc) and reverse (agtggaggtcctggaaactg), 776 bp; VGLUT2 forward (gcgcaaatctgtt aggagca) and reverse (ttttctcccagccgttagg), 816 bp; VGLUT3 forward (gctg gaccttctatttgctctta) and reverse (tctggtaggataatggctcctc), 759 bp; and nAChR α9 subunit forward (gtgggagtcctcgctgtctgcc) and reverse (gtgagtcccaggtgatg agccc), 490 bp. All PCR reactions were performed using the following touchdown protocol (40 cycles total): 94°C for 30 s, 60°C–50°C for 30 s with 1° decrease per cycle, 72°C for 1 min, followed by 94°C for 30 s, 50°C for 30 s, 72°C for 1 min (30 cycles), ending with a 10 min extension at 72°C, and storage at 4°C. The products were separated by electrophoresis through 2% agarose.

Auditory Testing

Acoustic startle responses of VGLUT3 KO (n = 7) and WT littermate (n = 7) mice were measured in darkened startle chambers (SR-LAB hardware and software, San Diego Instruments). Piezoelectric sensors located under the chambers detect and measure the peak startle response. Mice were acclimatized to the startle chambers by presentation of a 70 dB white noise for 5 min and then exposed to sound intensities of 80, 90, 100, 105, 110, 120, 125 dB (each with a 0 ms rise time, 40 ms plateau, 0 ms fall time), presented in pseudorandom order with intersound intervals of 10–50 s. Each run was repeated eight times. Average peak startle amplitude at each sound level was calculated from eight runs.

Auditory testing including auditory brainstem response (ABR) and distortion product otoacoustic emissions (DPOAEs) were done as previously described (Akil et al., 2006), with P21 VGLUT3 KO (n = 5), heterozygotes (n = 5), and WT littermates (n = 5) and P21 VGLUT1 KO mice (n = 4) (Fremeau et al., 2004a), heterozygotes (n = 5), and WT littermates (n = 4). For the compound action potential (CAP) recording, a ventral surgical approach (Jero et al., 2001) was used to expose the right cochlea of P14–17 VGLUT3 KO mice and WT littermates (n = 5). A fine Teflon-coated silver wire recording electrode was placed in the round window niche, and the ground electrode was placed in the soft tissue of the neck. The sound stimulus was generated with Tucker-Davis System II hardware and software (Tucker-Davis).

IHC and Afferent Fiber Recordings

After anesthesia with pentobarbital (0.045 mg/g i.p.), the dissected apical cochlear turns of 6- to 16-day-old VGLUT KO, WT littermates, and WT C57Bl/6 mice were placed into the chamber of an upright microscope, the IHCs and afferent nerve terminals visualized with 40× water-immersion objective and differential interference contrast optics, and the preparation superfused with saline at 1–3 ml/min. For isolating IHC Ca^{2+} currents, the pipette solution contained (in mM) $CsMeSO_3$ 135, TEA Cl 13, HEPES-CsOH 5 (pH 7.2), $MgCl_2$ 3.5, Na_2ATP 2.5, EGTA 1, and the extracellular solution KCl 5.8, NaCl 115.5, $MgCl_2$ 0.9, $CaCl_2$ 1.3, D-glucose 5.6, HEPES-NaOH 10 (pH 7.4), TEA Cl 30 as well as 4 mM 4-aminopyridine, 300 nM apamin, and 1 μM tetrodotoxin (Tocris Bioscience). The liquid junction potential (LJP) was −9 mV.

For the analysis of all IHC and afferent conductances other than Ca^{2+} currents, the pipette solution contained KCl 135, $MgCl_2$ 3.5, $CaCl_2$ 0.1, EGTA 5, HEPES-KOH 5, Na_2ATP 2.5; pH 7.2 (KOH) and the extracellular solution KCl 5.8, NaCl 155, $CaCl_2$ 1.3, NaH_2PO_4 0.7, glucose 5.6, HEPES-NaOH 10 (pH 7.4); LJP was −4 mV. Kainic acid, cyclothiazide, and NBQX (Tocris) were used at concentrations described in the text.

Recording pipettes were fabricated from 1 mm borosilicate glass, and fire polished with tip resistances of 10–15 (AF) and 4–5 (IHC) MΩ. Series resistance errors (5–11 MΩ) were not compensated for IHC Ca^{2+} currents and afferent fiber recordings, but were compensated 60%–95% on-line for 26 IHC recordings to characterize potassium conductances. For all IHC potassium conductances, voltages were corrected for the error across the uncompensated series resistance (<5 MΩ). Holding potentials were corrected off-line for LJPs. Recordings were made at 22°C–25°C with a Multiclamp 700A or 700B amplifier (Molecular Devices, Sunnyvale, CA) using pClamp version 9.2 or 10.2 and a Digidata 1322A board digitized at 50 kHz and filtered at 10 kHz. For leak subtraction, IHC membrane resistance was calculated from voltage

steps between −84 and −94 mV. For statistical comparison, one- or two-way ANOVA with Bonferroni post-tests (Graphpad Prism) were used. The data are presented as mean ± standard error (SE).

Electroencephalography

Chronic EEG electrodes were implanted in adult (3–7 month) VGLUT3 KO mice and WT littermates. Mice were anesthetized with 0.02 ml/g Avertin (1.25% tribromoethanol/amyl alcohol solution, i.p.). Teflon-coated silver wire electrodes (0.005 inch diameter) attached to a microminiature connector were implanted bilaterally into the subdural space over frontal, temporal, parietal, and occipital cortices. EEG activity was monitored daily during multiple, prolonged overnight and random 2 hr recording sessions for up to a total of 2 weeks (Stellate Systems, Harmonie software version 5.0b). A video camera was used to monitor behavior during the EEG recording periods. All recordings were carried out at least 24 hr after surgery on mice moving freely in the test cage.

Supplemental Data

The Supplemental Data for this article can be found online at http://www.neuron.org/cgi/content/full/57/2/263/DC1/.

ACKNOWLEDGMENTS

We thank Z. Hua, V. Nemani, and members of the Edwards laboratory for helpful discussion, the Epstein Laboratory, P. Leake, and G. Hradek in particular for critical advice and support on EM, H. Li-Korotky for assistance with initial ABR recordings, and I. Roux for help genotyping the VGLUT3 KO mice. R.P.S. was supported by NARSAD and NIMH; J.L.N. by NINDS and NICHD; K.K., E.G., and L.R.L. by NIDCD; L.G. by a grant to Paul Fuchs from NIDCD; and R.H.E. by NARSAD, NIMH, NIDA, and NINDS.

Received: July 2, 2007
Revised: October 26, 2007
Accepted: November 19, 2007
Published: January 23, 2008

REFERENCES

Abercrombie, M. (1946). Estimation of nuclear population from microtome sections. Anat. Rec. *94*, 239–247.

Akil, O., Chang, J., Hiel, H., Kong, J.H., Yi, E., Glowatzki, E., and Lustig, L.R. (2006). Progressive deafness and altered cochlear innervation in knock-out mice lacking prosaposin. J. Neurosci. *26*, 13076–13088.

Bobbin, R.P. (1979). Glutamate and aspartate mimic the afferent transmitter in the cochlea. Exp. Brain Res. *34*, 389–393.

Boulland, J.L., Qureshi, T., Seal, R.P., Rafiki, A., Gundersen, V., Bergersen, L.H., Fremeau, R.T., Jr., Edwards, R.H., Storm-Mathisen, J., and Chaudhry, F.A. (2004). Expression of the vesicular glutamate transporters during development indicates the widespread corelease of multiple neurotransmitters. J. Comp. Neurol. *480*, 264–280.

Brandt, A., Striessnig, J., and Moser, T. (2003). CaV1.3 channels are essential for development and presynaptic activity of cochlear inner hair cells. J. Neurosci. *23*, 10832–10840.

Brandt, N., Kuhn, S., Munkner, S., Braig, C., Winter, H., Blin, N., Vonthein, R., Knipper, M., and Engel, J. (2007). Thyroid hormone deficiency affects postnatal spiking activity and expression of Ca2+ and K+ channels in rodent inner hair cells. J. Neurosci. *27*, 3174–3186.

Cobos, I., Calcagnotto, M.E., Vilaythong, A.J., Thwin, M.T., Noebels, J.L., Baraban, S.C., and Rubenstein, J.L. (2005). Mice lacking Dlx1 show subtype-specific loss of interneurons, reduced inhibition and epilepsy. Nat. Neurosci. *8*, 1059–1068.

Comis, S.D., and Leng, G. (1979). Action of putative neurotransmitters in the guinea pig cochlea. Exp. Brain Res. *36*, 119–128.

Croft, B.G., Fortin, G.D., Corera, A.T., Edwards, R.H., Beaudet, A., Trudeau, L.E., and Fon, E.A. (2005). Normal biogenesis and cycling of empty synaptic vesicles in dopamine neurons of vesicular monoamine transporter 2 knockout mice. Mol. Biol. Cell *16*, 306–315.

Daniels, R.W., Collins, C.A., Chen, K., Gelfand, M.V., Featherstone, D.E., and Diantonio, A. (2006). A single vesicular glutamate transporter is sufficient to fill a synaptic vesicle. Neuron *49*, 11–16.

Eglen, S.J., Demas, J., and Wong, R.O. (2003). Mapping by waves. Patterned spontaneous activity regulates retinotopic map refinement. Neuron *40*, 1053–1055.

Eybalin, M., Caicedo, A., Renard, N., Ruel, J., and Puel, J.L. (2004). Transient Ca2+-permeable AMPA receptors in postnatal rat primary auditory neurons. Eur. J. Neurosci. *20*, 2981–2989.

Firth, S.I., Wang, C.T., and Feller, M.B. (2005). Retinal waves: mechanisms and function in visual system development. Cell Calcium *37*, 425–432.

Fon, E.A., Pothos, E.N., Sun, B.-C., Killeen, N., Sulzer, D., and Edwards, R.H. (1997). Vesicular transport regulates monoamine storage and release but is not essential for amphetamine action. Neuron *19*, 1271–1283.

Fremeau, R.T., Jr., Troyer, M.D., Pahner, I., Nygaard, G.O., Tran, C.H., Reimer, R.J., Bellocchio, E.E., Fortin, D., Storm-Mathisen, J., and Edwards, R.H. (2001). The expression of vesicular glutamate transporters defines two classes of excitatory synapse. Neuron *31*, 247–260.

Fremeau, R.T., Jr., Burman, J., Qureshi, T., Tran, C.H., Proctor, J., Johnson, J., Zhang, H., Sulzer, D., Copenhagen, D.R., Storm-Mathisen, J., et al. (2002). The identification of vesicular glutamate transporter 3 suggests novel modes of signaling by glutamate. Proc. Natl. Acad. Sci. USA *99*, 14488–14493.

Fremeau, R.T., Jr., Kam, K., Qureshi, T., Johnson, J., Copenhagen, D.R., Storm-Mathisen, J., Chaudhry, F.A., Nicoll, R.A., and Edwards, R.H. (2004a). Vesicular glutamate transporters 1 and 2 target to functionally distinct synaptic release sites. Science *304*, 1815–1819.

Fremeau, R.T., Jr., Voglmaier, S., Seal, R.P., and Edwards, R.H. (2004b). VGLUTs define subsets of excitatory neurons and suggest novel roles for glutamate. Trends Neurosci. *27*, 98–103.

Furness, D.N., and Lawton, D.M. (2003). Comparative distribution of glutamate transporters and receptors in relation to afferent innervation density in the mammalian cochlea. J. Neurosci. *23*, 11296–11304.

Gillespie, D.C., Kim, G., and Kandler, K. (2005). Inhibitory synapses in the developing auditory system are glutamatergic. Nat. Neurosci. *8*, 332–338.

Glowatzki, E., and Fuchs, P.A. (2002). Transmitter release at the hair cell ribbon synapse. Nat. Neurosci. *5*, 147–154.

Gras, C., Herzog, E., Bellenchi, G.C., Bernard, V., Ravassard, P., Pohl, M., Gasnier, B., Giros, B., and El Mestikawy, S. (2002). A third vesicular glutamate transporter expressed by cholinergic and serotoninergic neurons. J. Neurosci. *22*, 5442–5451.

Gras, C., Vinatier, J., Amilhon, B., Guerci, A., Christov, C., Ravassard, P., Giros, B., and El Mestikawy, S. (2005). Developmentally regulated expression of VGLUT3 during early post-natal life. Neuropharmacology *49*, 901–911.

Griesinger, C.B., Richards, C.D., and Ashmore, J.F. (2002). Fm1-43 reveals membrane recycling in adult inner hair cells of the mammalian cochlea. J. Neurosci. *22*, 3939–3952.

Griesinger, C.B., Richards, C.D., and Ashmore, J.F. (2005). Fast vesicle replenishment allows indefatigable signalling at the first auditory synapse. Nature *435*, 212–215.

Harkany, T., Holmgren, C., Hartig, W., Qureshi, T., Chaudhry, F.A., Storm-Mathisen, J., Dobszay, M.B., Berghuis, P., Schulte, G., Sousa, K.M., et al. (2004). Endocannabinoid-independent retrograde signaling at inhibitory synapses in layer 2/3 of neocortex: involvement of vesicular glutamate transporter 3. J. Neurosci. *24*, 4978–4988.

Hegarty, J.L., Kay, A.R., and Green, S.H. (1997). Trophic support of cultured spiral ganglion neurons by depolarization exceeds and is additive with that by neurotrophins or cAMP and requires elevation of [Ca2+]i within a set range. J. Neurosci. *17*, 1959–1970.

Herzog, E., Bellenchi, G.C., Gras, C., Bernard, V., Ravassard, P., Bedet, C., Gasnier, B., Giros, B., and El Mestikaway, S. (2001). The existence of a second

vesicular glutamate transporter specifies subpopulations of glutamatergic neurons. J. Neurosci. *21*, RC181.

Hioki, H., Fujiyama, F., Nakamura, K., Wu, S.X., Matsuda, W., and Kaneko, T. (2004). Chemically specific circuit composed of vesicular glutamate transporter 3- and preprotachykinin B-producing interneurons in the rat neocortex. Cereb. Cortex *14*, 1266–1275.

Jero, J., Tseng, C.J., Mhatre, A.N., and Lalwani, A.K. (2001). A surgical approach appropriate for targeted cochlear gene therapy in the mouse. Hear. Res. *151*, 106–114.

Johnson, J., Tian, N., Caywood, M.S., Reimer, R.J., Edwards, R.H., and Copenhagen, D.R. (2003). Vesicular neurotransmitter transporter expression in developing postnatal rodent retina: GABA and glycine precede glutamate. J. Neurosci. *23*, 518–529.

Johnson, S.L., Marcotti, W., and Kros, C.J. (2005). Increase in efficiency and reduction in Ca2+ dependence of exocytosis during development of mouse inner hair cells. J. Physiol. *563*, 177–191.

Kaneko, T., Fujiyama, F., and Hioki, H. (2002). Immunohistochemical localization of candidates for vesicular glutamate transporters in the rat brain. J. Comp. Neurol. *444*, 39–62.

Katz, E., Elgoyhen, A.B., Gomez-Casati, M.E., Knipper, M., Vetter, D.E., Fuchs, P.A., and Glowatzki, E. (2004). Developmental regulation of nicotinic synapses on cochlear inner hair cells. J. Neurosci. *24*, 7814–7820.

Khimich, D., Nouvian, R., Pujol, R., Tom Dieck, S., Egner, A., Gundelfinger, E.D., and Moser, T. (2005). Hair cell synaptic ribbons are essential for synchronous auditory signalling. Nature *434*, 889–894.

Knipper, M., Kopschall, I., Rohbock, K., Kopke, A.K., Bonk, I., Zimmermann, U., and Zenner, H. (1997). Transient expression of NMDA receptors during rearrangement of AMPA-receptor-expressing fibers in the developing inner ear. Cell Tissue Res. *287*, 23–41.

Kros, C.J., Ruppersberg, J.P., and Rusch, A. (1998). Expression of a potassium current in inner hair cells during development of hearing in mice. Nature *394*, 281–284.

Lenzi, D., Crum, J., Ellisman, M.H., and Roberts, W.M. (2002). Depolarization redistributes synaptic membrane and creates a gradient of vesicles on the synaptic body at a ribbon synapse. Neuron *36*, 649–659.

Marcotti, W., Johnson, S.L., Rusch, A., and Kros, C.J. (2003). Sodium and calcium currents shape action potentials in immature mouse inner hair cells. J. Physiol. *552*, 743–761.

Miyazaki, T., Fukaya, M., Shimizu, H., and Watanabe, M. (2003). Subtype switching of vesicular glutamate transporters at parallel fibre-Purkinje cell synapses in developing mouse cerebellum. Eur. J. Neurosci. *17*, 2563–2572.

Moechars, D., Weston, M.C., Leo, S., Callaerts-Vegh, Z., Goris, I., Daneels, G., Buist, A., Cik, M., van der Spek, P., Kass, S., et al. (2006). Vesicular glutamate transporter VGLUT2 expression levels control quantal size and neuropathic pain. J. Neurosci. *26*, 12055–12066.

Moser, T., and Beutner, D. (2000). Kinetics of exocytosis and endocytosis at the cochlear inner hair cell afferent synapse of the mouse. Proc. Natl. Acad. Sci. USA *97*, 883–888.

Nemzou, N.R., Bulankina, A.V., Khimich, D., Giese, A., and Moser, T. (2006). Synaptic organization in cochlear inner hair cells deficient for the CaV1.3 (alpha1D) subunit of L-type Ca2+ channels. Neuroscience *141*, 1849–1860.

Noebels, J.L., and Sidman, R.L. (1979). Inherited epilepsy: spike-wave and focal motor seizures in the mutant mouse tottering. Science *204*, 1334–1336.

Ottersen, O.P., Takumi, Y., Matsubara, A., Landsend, A.S., Laake, J.H., and Usami, S. (1998). Molecular organization of a type of peripheral glutamate synapse: the afferent synapses of hair cells in the inner ear. Prog. Neurobiol. *54*, 127–148.

Platzer, J., Engel, J., Schrott-Fischer, A., Stephan, K., Bova, S., Chen, H., Zheng, H., and Striessnig, J. (2000). Congenital deafness and sinoatrial node dysfunction in mice lacking class D L-type Ca2+ channels. Cell *102*, 89–97.

Pyott, S.J., Glowatzki, E., Trimmer, J.S., and Aldrich, R.W. (2004). Extrasynaptic localization of inactivating calcium-activated potassium channels in mouse inner hair cells. J. Neurosci. *24*, 9469–9474.

Roux, I., Safieddine, S., Nouvian, R., Grati, M., Simmler, M.C., Bahloul, A., Perfettini, I., Le Gall, M., Rostaing, P., Hamard, G., et al. (2006). Otoferlin, defective in a human deafness form, is essential for exocytosis at the auditory ribbon synapse. Cell *127*, 277–289.

Rusch, A., Ng, L., Goodyear, R., Oliver, D., Lisoukov, I., Vennstrom, B., Richardson, G., Kelley, M.W., and Forrest, D. (2001). Retardation of cochlear maturation and impaired hair cell function caused by deletion of all known thyroid hormone receptors. J. Neurosci. *21*, 9792–9800.

Safieddine, S., and Wenthold, R.J. (1999). SNARE complex at the ribbon synapses of cochlear hair cells: analysis of synaptic vesicle- and synaptic membrane-associated proteins. Eur. J. Neurosci. *11*, 803–812.

Schafer, M.K., Varoqui, H., Defamie, N., Weihe, E., and Erickson, J.D. (2002). Molecular cloning and functional identification of mouse vesicular glutamate transporter 3 and its expression in subsets of novel excitatory neurons. J. Biol. Chem. *277*, 50734–50748.

Sendin, G., Bulankina, A.V., Riedel, D., and Moser, T. (2007). Maturation of ribbon synapses in hair cells is driven by thyroid hormone. J. Neurosci. *27*, 3163–3173.

Shatz, C.J. (1996). Emergence of order in visual system development. Proc. Natl. Acad. Sci. USA *93*, 602–608.

Sherry, D.M., Wang, M.M., Bates, J., and Frishman, L.J. (2003). Expression of vesicular glutamate transporter 1 in the mouse retina reveals temporal ordering in development of rod vs. cone and ON vs. OFF circuits. J. Comp. Neurol. *465*, 480–498.

Simmons, D.D. (2002). Development of the inner ear efferent system across vertebrate species. J. Neurobiol. *53*, 228–250.

Simmons, D.D., Mansdorf, N.B., and Kim, J.H. (1996). Olivocochlear innervation of inner and outer hair cells during postnatal maturation: evidence for a waiting period. J. Comp. Neurol. *370*, 551–562.

Somogyi, J., Baude, A., Omori, Y., Shimizu, H., Mestikawy, S.E., Fukaya, M., Shigemoto, R., Watanabe, M., and Somogyi, P. (2004). GABAergic basket cells expressing cholecystokinin contain vesicular glutamate transporter type 3 (VGLUT3) in their synaptic terminals in hippocampus and isocortex of the rat. Eur. J. Neurosci. *19*, 552–569.

Soriano, P., Montgomery, C., Geske, R., and Bradley, A. (1991). Targeted disruption of the c-src proto-oncogene leads to osteopetrosis in mice. Cell *64*, 693–702.

Takamori, S. (2006). VGLUTs: 'exciting' times for glutamatergic research? Neurosci. Res. *55*, 343–351.

Takamori, S., Rhee, J.S., Rosenmund, C., and Jahn, R. (2000). Identification of a vesicular glutamate transporter that defines a glutamatergic phenotype in neurons. Nature *407*, 189–194.

Takamori, S., Rhee, J.S., Rosenmund, C., and Jahn, R. (2001). Identification of differentiation-associated brain-specific phosphate transporter as a second vesicular glutamate transporter. J. Neurosci. *21*, RC182.

Thomas, K.R., and Capecchi, M.R. (1987). Site-directed mutagenesis by gene targeting in mouse embryo-derived stem cells. Cell *51*, 503–512.

Tordera, R.M., Totterdell, S., Wojcik, S.M., Brose, N., Elizalde, N., Lasheras, B., and Del Rio, J. (2007). Enhanced anxiety, depressive-like behaviour and impaired recognition memory in mice with reduced expression of the vesicular glutamate transporter 1 (VGLUT1). Eur. J. Neurosci. *25*, 281–290.

Tybulewicz, V.L., Crawford, C.E., Jackson, P.K., Bronson, R.T., and Mulligan, R.C. (1991). Neonatal lethality and lymphopenia in mice with a homozygous disruption of the c-abl proto-oncogene. Cell *65*, 1153–1163.

Varoqui, H., Schafer, M.K.-H., Zhu, H., Weihe, E., and Erickson, J.D. (2002). Identification of the differentiation-associated Na+/Pi transporter as a novel vesicular glutamate transporter expressed in a distinct set of glutamatergic synapses. J. Neurosci. *22*, 142–155.

Voglmaier, S.M., Kam, K., Yang, H., Fortin, D.L., Hua, Z., Nicoll, R.A., and Edwards, R.H. (2006). Distinct endocytic pathways control the rate and extent of synaptic vesicle protein recycling. Neuron *51*, 71–84.

Wojcik, S.M., Rhee, J.S., Herzog, E., Sigler, A., Jahn, R., Takamori, S., Brose, N., and Rosenmund, C. (2004). An essential role for vesicular glutamate transporter 1 (VGLUT1) in postnatal development and control of quantal size. Proc. Natl. Acad. Sci. USA *101*, 7158–7163.

Yasunaga, S., Grati, M., Cohen-Salmon, M., El-Amraoui, A., Mustapha, M., Salem, N., El-Zir, E., Loiselet, J., and Petit, C. (1999). A mutation in OTOF, encoding otoferlin, a FER-1-like protein, causes DFNB9, a nonsyndromic form of deafness. Nat. Genet. *21*, 363–369.